Rapid Fabrication of Precise, High-Throughput Filters from Membrane Protein Nanosheets

Yu-Ming Tu^{1,†}, Woochul Song^{1,†}, Tingwei Ren^{1,†}, Yuexiao Shen², Ratul Chowdhury¹, Prasangi Rajapaksha³, Tyler E. Culp¹, Laxmicharan Samineni¹, Lang Chao^{1,4}, Alina Thokkadam⁵, Drew Carson¹, Yuxuan Dai¹, Arwa Mukthar⁶, Miaoci Zhang¹, Andrey Parshin⁷, Mariusz Grzelakowski⁷, Dibakar Bhattacharya⁸, William A. Phillip⁹, Enrique D. Gomez¹, Robert J. Hickey^{4,10}, Yinai Wei³, and Manish Kumar^{1,11,12,*}

Tel.: (814)-865-7519

e-mail: manish.kumar@psu.edu

†These authors contributed equally to this work.

¹Department of Chemical Engineering, ⁴Department of Material Science and Engineering, ⁶Department of Biochemistry and Molecular Biology, ¹⁰the Materials Research Institute, ¹¹Department of Civil and Environmental Engineering, ¹²Department of Biomedical Engineering, Pennsylvania State University, University Park, PA16802, USA

²Department of Chemistry, University of California, Berkeley, CA 94720, USA

³Department of Chemistry, ⁸Department of Chemical and Materials Engineering, University of Kentucky, Lexington, KY 40506, USA

⁵Department of Chemical & Biochemical Engineering, Rutgers University, Piscataway, NJ 08854, USA ⁷Applied Biomimetic, Gaithersburg, MD, 20878, USA

⁹Department of Chemical and Biomolecular Engineering, University of Notre Dame, Notre Dame, IN 46556, USA

^{*}To whom correspondence should be addressed

Abstract

Biological membranes are ideal for separations as they provide high permeability while maintaining high solute selectivity due to the presence of specialized membrane protein (MP) channels. Several biological membranes also exhibit high channel packing densities, sometimes in the form of two-dimensional (2D) arrays or crystals. Despite numerous attempts, successful integration of MPs into practical membranes has remained a significant challenge. Here, we present an efficient method of preparing 2D crystals and nanosheets of highly packed pore-forming MPs in block copolymers. We then demonstrate the integration of these unique hybrid materials into scalable protein-copolymer biomimetic membranes. These protein nanosheet membranes maintain the molecular selectivity of the three types of β -barrel MPs used, with pore sizes of 0.8 nm, 1.3 nm and 1.5 nm. These biomimetic membranes demonstrate 20-1,000 times greater water permeability than commercial membranes and 1.5-45 times than that of the latest research membranes with comparable molecular exclusion ratings, thus providing a superior alternative in the challenging sub-nm to few-nm size range.

Biological membrane protein (MP) channels¹⁻⁴, synthetic channels⁵⁻⁸, and carbon nanotubes⁹ have emerged as promising platforms for the development of separation membranes with precise molecular selectivity¹⁰. Relative to state-of-the-art commercial membranes^{11, 12}, biomimetic membranes incorporating these pore structures are expected to exhibit high permeability and selectivity because they possess a high density of channels with a well-defined pore geometry and functionality designed to exclude or pass specific components from complicated mixtures^{3, 13}. MP-based biomimetic membranes studied thus far have been limited to small improvements in performance that are much lower than the orders of magnitude enhancement anticipated from early experiments¹. Current MP-based biomimetic membranes show 2-3× increases in permeability over commercial membranes 14, 15 with similar or worse selectivity. This has been attributed to the use of vesicular morphologies of channel-reconstituted liposomes 15-17 and the low protein content 3, 18, 19 in biomimetic matrices used for membrane fabrication. In addition, widespread application of MP-based biomimetic membranes developed so far may be limited due to the use of non-scalable fabrication techniques used for membrane synthesis (e.g., detergent removal-based self-assembly techniques)^{10, 20}. Designing membranes with high packing densities of channel proteins with uniform pore sizes of ~0.5-1.5 nm with less material- and time-intensive synthesis techniques could provide a path to meet the ultimate promise of biomimetic membranes in this important solute size range^{13, 20}.

Channel proteins can be regarded as ideal pore geometries because they exhibit transport properties targeted towards specific small molecule separations, which are necessary to maintain cellular functions²¹. *In vivo*, passive β -barrel channel proteins are used for the exclusion of large molecules (such as proteins) while allowing or inducing ion and small molecule permeation (e.g., sugars and antibiotics)²². The stability and mutation tolerance of β -barrel proteins make them ideal candidates for the development of channel protein-based membranes². Additionally, the β -barrel structure is a robust scaffold with high thermodynamic stability^{23, 24}, and can be incorporated in an oriented and functionally-active form within lipid bilayers²⁵ and amphiphilic polymers²⁶⁻²⁸ demonstrated as trigonal or tetragonal crystal structures^{29, 30}. Their high structural stability can be attributed to the low enthalpies of denaturation of the transmembrane domains^{31, 32}. These precisely-sized and stable protein channels were used in this work for the scalable fabrication of high performance biomimetic membranes¹⁹.

We present a comprehensive approach to construct biomimetic membranes beginning with the scalable synthesis of two-dimensional (2D) crystals and nanosheets that contain a high packing density of β -barrel proteins. (**Fig. 1**). The membranes fabricated from these 2D materials showed significant improvements in membrane productivity (water permeability) and maintained designed selectivity as a result of the high porosities and unitary pore shapes of the protein channels. Three different pore-forming β -barrel channel proteins, outer membrane protein F (OmpF)³³, a mutated version of a bacterial ferrichrome outer membrane transporter (designated FhuA $\Delta C/\Delta 4L$)^{16, 34}, and a channel forming protein toxin from *Staphylococcus aureus*, alpha-hemolysin (α HL)³⁵, were selected to demonstrate this approach. These proteins possess unique elliptical or cylindrical pore dimensions of 0.8×1.08 nm, 1.31×1.62 nm, and 1.50×1.50 nm for OmpF, FhuA $\Delta C/\Delta 4L$, and α HL, respectively (**Fig. 1a**, also see Supplementary Information for pore size evaluation details). Simultaneously achieving precise control over pore sizes in this range, while maintaining uniformity in pore size and achieving a high porosity, is quite difficult using current membranes. MP 2D crystal arrays or nanosheets were created by reconstituting these channel proteins into

poly(butadiene)-b-poly(ethylene oxide) (PB-PEO) di-block copolymers (BCPs) through two selfassembly strategies: detergent removal by dialysis (dialysis method) and self-assembly from BCP-MP films deposited using organic solvent evaporation (solvent method) (Fig. 1b). The dialysis method is known to be capable of assembling protein and artificial water channels into ordered 2D crystal arrays^{1, 28, 36} and artificial channels into highly packed 2D nanosheets³⁷. However, this "slow dialysis" method takes ~6 days to complete and translating such a time-intensive process to larger scales is not practical. In this work, we introduce a unique solvent-based method for the preparation of 2D protein channel nanosheets. The surprising success in formation of nanosheets and 2D crystals of channel proteins with BCPs by the solvent method resulted in a significant decrease in the process time from 6 days to ~2 hours. Moreover, it had the added benefit of reducing the usage of MP-compatible detergent, which is often a high-cost specialty chemical³⁸. The prepared 2D crystals or nanosheets were deposited onto commercial porous support membranes using a layer-by-layer technique³⁷ to form continuous and defect-free selective layers (Fig. 1c). Water permeability of all tested channel-based membranes showed orders of magnitude improvements (20-1000x) over current polymeric nanofiltration (NF) membranes with comparable molecular exclusion ratings. These permeabilities were 293 ± 51 L m⁻² h⁻¹ bar⁻¹ (denoted as LMH bar⁻¹), 793 ± 226 LMH bar⁻¹, and $2{,}107 \pm 235$ LMH bar⁻¹ (all values mean \pm s.d., $n \ge 3$) for OmpF, FhuA $\Delta C/\Delta 4L$, and αHL -based biomimetic membranes, respectively. Additionally, these membranes exhibit the molecular exclusion performance inferred from their structures with molecular weight cut-offs (MWCOs) of ~480, ~1,130, and ~930 Da for OmpF, FhuA $\Delta C/\Delta 4L$, and αHL -based membranes, respectively. These results demonstrate the potential of utilizing β-barrel channel proteins to tailor membrane selectivity within a critical separation range, while realizing high permeability enhancement.

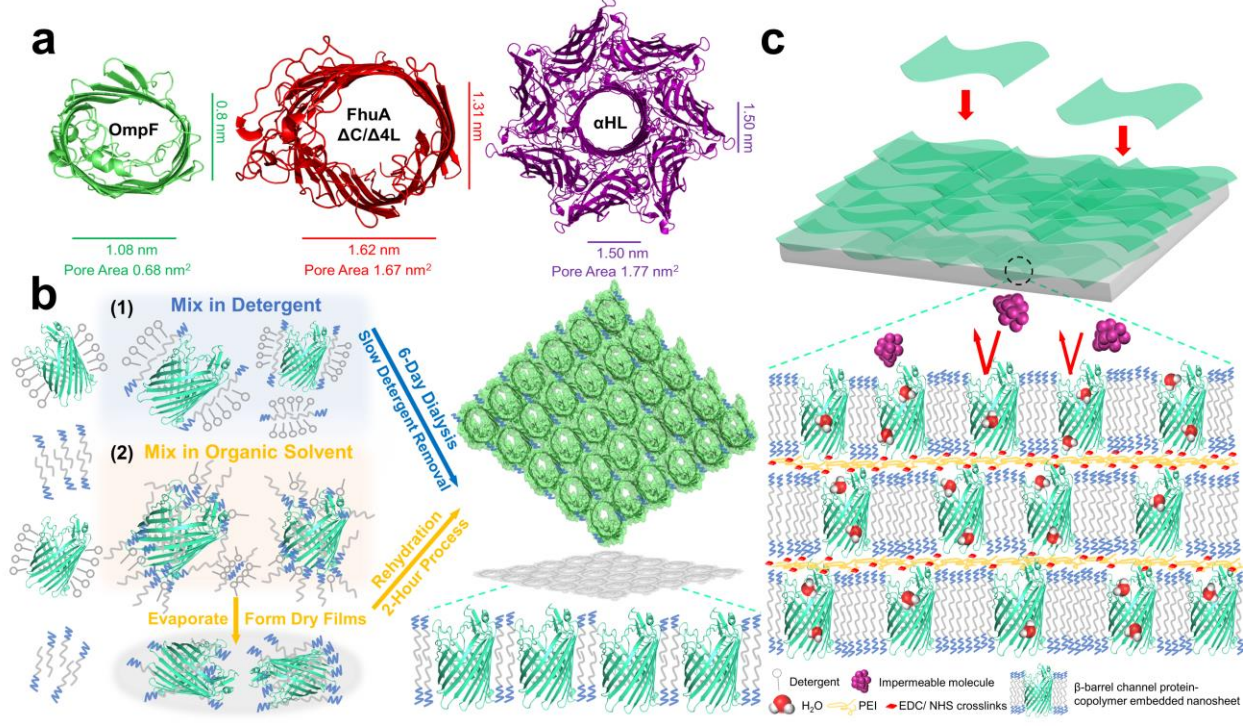


Fig. 1 | **Stable** β-barrel channel protein-polymer-based scalable membranes. a, Three distinct β-barrel channel proteins were used: (i) OmpF from *E. coli* (PDB: 2OMF) that excludes proteins but allows small sugars, nutrients and antibiotics to pass through, with *in silico* estimated pore sizes of 0.8×1.08 nm, (ii) FhuA $\Delta C/\Delta 4L$ from *E. coli* that originally forms part of a larger pore complex for active ferrichrome-iron and antibiotic transports but is engineered with its central alpha-helical plug removed as a passive pore in this work, resultant pore size of 1.31×1.62 nm, (iii) alpha hemolysin, a self-assembled structure created by *Staphylococcus aureus* to porate cell membranes, with an estimated pore size of 1.50×1.50 nm (PDB: 7AHL) b, Two self-assembly methods to construct high density 2D β-barrel channel protein-BCP crystals or nanosheets by self-assembly using (1) detergent dialysis method, a slow detergent removal process with a 6-day dialysis process, and (2) organic solvent extraction method, a 2-hour self-assembly process with addition of chloroform and methanol mixture to protein and polymers, then solvent evaporation, followed by aqueous rehydration. (c) Schematic illustration of the layer-by-layer membrane fabrication procedure with densely packed β-barrel channel protein-BCP nanosheets on porous substrates. These scalable channel protein-incorporated biomimetic membranes achieved precise molecular selectivity while demonstrating high water permeability.

Results and Discussions

Reconstitution of β-barrel protein channels into porous 2D nanosheets

2D materials with uniformly-sized internal pores have various advantages in terms of membrane development. Porous sheet-like structures can be used to form defect-free but thin selective layers that lead to high productivity¹⁹. Unitary pore structures can provide desirable molecular selectivity properties based primarily on molecular sieving effects.

Three pore-forming β -barrel membrane proteins, OmpF, FhuA $\Delta C/\Delta 4L$, and αHL , were selected based on their unique pore dimensions of 0.8×1.08 nm, 1.31×1.62 nm, and 1.50×1.50 nm, respectively, and reconstituted into 2D porous nanosheet structures. Amphiphilic PB-PEO BCPs were used as membrane matrices due to their higher chemical and mechanical stability compared to native lipids^{36, 39-41} as well as their physical and chemical compatibility for membrane protein insertion^{3, 42}. We first used a dialysis-based method for the formation of 2D nanosheet structures. In this method, the assembly kinetics of the proteins and BCPs are controlled through the gradual removal of high concentrations of detergents from a ternary mixture of protein, BCP, and detergent via dialysis (Fig.1b (1))^{1, 28, 37}. Assembly of OmpF proteins and PB-PEO BCPs using this method resulted in hexagonally-packed 2D protein crystals at protein to polymer ratios (PoPR, w/w) of 0.2-0.6, similar to that reported in our previous study²⁸. As observed by negative-stain transmission electron microscopy (TEM), micron-scale BCP-OmpF crystals were formed using the dialysis methods (Fig. 2a). Fast Fourier transform (FFT) analysis of the electron diffraction pattern from TEM with the Focus software⁴³ (Fig. 2b) identified a hexagonal unit cell with lattice dimensions of a = b = 18 nm and $\gamma = 120^{\circ}$. These dimensions are similar to those reported in our previous study on BCP- OmpF 2D crystals²⁸ and indicates a pore packing density of ~3.2×10⁴ pores µm⁻². This pore density represents the ultimate packing density of OmpF in block copolymers and demonstrates that the protocols we use for MPs leads to a high performance material and provides a way to get over the limited packing density of $\sim 10^3$ pores μm^{-2} in vesicle-based systems. A similar dialysis protocol was also applied to FhuA $\Delta C/\Delta 4L$ and αHL proteins with PoPR of 0.2-0.35 and 0.25-0.4, respectively, in order to prepare highly packed MP-BCP 2D nanosheets. As shown in Fig. 2e and f, both FhuA $\Delta C/\Delta 4L$ and αHL proteins were successfully integrated into 2D nanosheet structures. No evidence of crystallinity was seen for these two proteins.

Removing detergents via dialysis is a well-established, but slow method of preparing MP 2D crystals and nanosheets in lipids^{44, 45} and more recently in polymers²⁸. Generally, this process

takes $3\sim6$ days to be completed^{28, 42, 46}. Furthermore, MP-BCP 2D crystal formation by dialysis⁴² requires a large amount of specialty non-ionic detergent per preparation, which could be a factor limiting the scalability of this technique³⁸. Hence, to shorten the time required for 2D nanosheet assembly and minimize the usage of detergents, we explored a new approach to prepare 2D protein crystals and nanosheets, which is referred to as the solvent method in this work. This new approach was inspired by reports on the extraction of hydrophobic membrane proteins from native cell membranes using organic solvents⁴⁷. The high stability of the β -barrel structure also provided an impetus to pursue the development of this technique, which relies on the hypothesis that the β -barrel proteins used would maintain their structure when exposed to solvents during the short processing time utilized. While not needed in this effort, a different β -barrel protein was mutated to improve its thermal and solvent stability⁴⁸ indicating that the solvent resistance of these proteins can be even further evolved, if needed, in future implementations.

The solvent method utilized included three steps: (1) mixing proteins and BCPs in a methanol/chloroform (MeOH/CHCl₃) mixture (50% v/v) at specific PoPRs, (2) evaporating solvents to form protein/BCP films on glass surfaces, and (3) rehydrating the protein-BCP films using aqueous buffer solutions (Fig.1b (2)). The hydrophobic outer surfaces of the selected MPs allowed them to be readily dissolved in the MeOH/CHCl₃ solvent mixture. We propose that, upon addition of BCPs dissolved in organic solvents to the protein solution, the hydrophilic surfaces of the β-barrel proteins were associated with hydrophilic PEO blocks and protected from the organic solvent environment by the hydrophobic PB block. This is similar to the protein stabilizing mechanism demonstrated in a recent study on protecting protein structure and function in organic solvents through the use of heteropolymers containing random hydrophobic and hydrophilic blocks of predefined domain sizes⁴⁹. During the solvent evaporation step, the polymer/BCP are mixed with detergent containing MPs to form films containing detergent, BCP and MPs. Subsequent film rehydration enables detergents to be diluted below their critical micelle concentration (CMC), allowing them to escape from protein/BCP/detergent complexes to the aqueous buffer solution. This detergent removal likely induces MP-BCP re-orientation into assembled 2D structures. We propose that when the dry polymer stabilized membrane protein film containing a small amount of detergent is hydrated in aqueous buffer, the detergent is diluted to much below its CMC leading to a similar self-assembly process as is seen with the detergent dialysis method. It is unclear why in this case the process is so rapid while in the dialysis based detergent removal process, the detergent removal kinetics need to be much slower according to previous studies⁵⁰. The solvent method required just ~2 hours with much lower detergent use and is thus more time and resource efficient. The elimination of detergent use during membrane assembly is an important step towards making 2D crystal/nanosheet biomimetic membranes more economical as membrane protein compatible detergents are major cost components of biomimetic membranes³⁸.

The success of using the solvent method in the preparation of porous protein nanosheets was confirmed by TEM analysis. OmpF-BCP nanosheets prepared using the solvent method showed identical crystal forms to the OmpF crystals (hexagonal unit cells as inferred from the FFT patterns) prepared using the dialysis method (**Fig. 2d**). Successful formation of nanosheets of α HL and FhuA Δ C/ Δ 4L proteins was also identified by TEM analysis as shown in **Fig. 2f** and **Supplementary Fig. 1**.

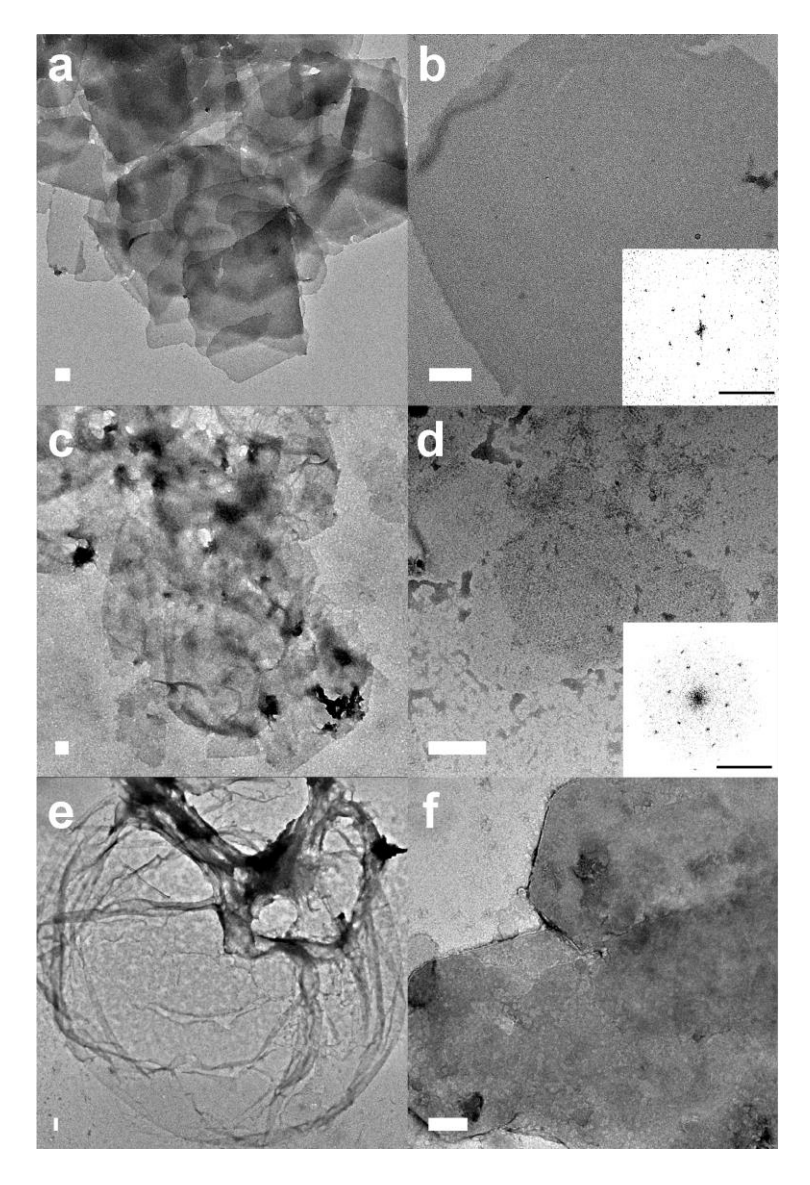


Fig. 2 | 2D crystals or nanosheets of three β-barrel channel proteins reconstituted in BCP membrane matrices. Negative-stain transmission electron microscopy (TEM) images of OmpF 2D crystals prepared by $\bf a$, dialysis and $\bf c$, solvent method illustrates the characteristic morphologies of microscale 2D flat nanosheets. TEM images at high magnification with diffraction spots (insets) by fast Fourier transformation (FFT) of OmpF crystal images formed by $\bf b$, dialysis and $\bf d$, solvent method reveal the high degree of protein incorporation and crystalline structures. Negative-stain TEM images of $\bf e$, αHL nanosheets and $\bf f$, FhuA $\Delta C/\Delta 4$ L constructed by a dialysis method demonstrate 2D nanosheet formation. The scale bar is 100 nm and the scale bar in the insets is 10 nm^{-1} .

Integrity of pore-forming β -barrel protein structures in crystals formed from the MP-BCP-MeOH/CHCl3 solvent mixtures

Preserving the structures of pore-forming β -barrel sheets, after processing in MeOH/CHCl₃ solvent mixtures was of critical importance, because denatured proteins may lose the unique pore

structures that form the basis of this work. Circular dichroism (CD) spectroscopy was performed to confirm that the structural integrity of the three protein channels was retained after nanosheet formation via the solvent method process.⁵¹ Nanosheets formed by the more established dialysis method were also characterized for comparison. As shown in Fig. 3a, the CD spectra of OmpF detergent-solubilized proteins revealed a positive peak near 200 nm and a negative peak around 220 nm, reflecting the predominantly β-sheet structure of the protein⁵². For OmpF 2D crystals prepared by the dialysis and solvent method, similar representative peaks were observed near 220 nm, qualitatively suggesting that the β-barrel structure of OmpF was similarly maintained throughout both crystallization processes. Specifically, CD spectra peaks were shown to be redshifted from purified proteins (216.8 nm), to crystals (dialysis method: 218.4 nm and solvent method: 220 nm). These shifts are expected due to the highly-aligned configurations of the β-barrel sheet structures within the 2D crystals. This phenomenon is also seen in the crystal structure of E.coli OmpF porins obtained in lipidic cubic phases (3POQ) (at 221 nm)^{53, 54} (Fig. 3a and Supplementary Fig. 2). This slight red shift of the peak position could be attributed to absorption flattening optical effects that are a consequence of the ordered distribution of peptides within a crystalline structure^{52,55}. The protein secondary structure content was estimated by fitting CD spectra with JWMVS-529 Multivariate SSE analysis program with 26 reference proteins. The structural content of OmpF (Supplementary Table 1) indicates that β-sheet content of OmpF 2D crystals in BCPs increases compared to that of OmpF proteins in detergent and is close to that of lipidic cubic phase OmpF crystals (3POQ). This implies that OmpF 2D crystals not only preserve β-barrel structures after crystallization but also organize OmpF proteins into ordered and large aggregates in BCP membrane matrices. The peak position occurring at less than ~200 nm could not be characterized owing to the strong absorption at shorter wavelengths from the rehydration buffer (10 mM Tris, 1.2% OG, pH7.4) we used for crystallization (Supplementary Fig. 3). As shown in Figs. 3b, c, the secondary structure analysis of FhuA $\Delta C/\Delta 4L$ and αHL CD spectra also provides confidence that nanosheet assembly by both solvent and dialysis method can conserve βsheet structures similarly. The secondary structure of FhuA ΔC/Δ4L-BCP and αHL-BCP nanosheets prepared by solvent and dialysis method showed higher percentage of β-sheet content than that of FhuA $\Delta C/\Delta 4L$ and αHL in detergent micelles, indicating a high packing density of proteins in BCP membrane matrix (Supplementary Table 1).

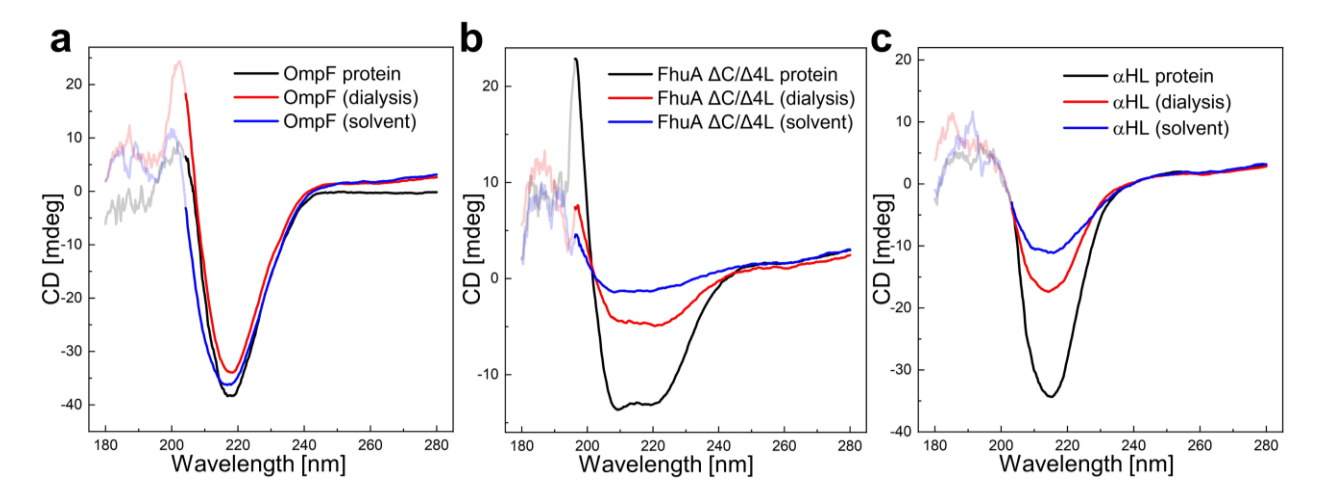


Fig. 3 | Circular dichroism spectroscopy (CD) results of β -barrel channel protein (black line) and protein-copolymer crystals or nanosheets using a dialysis (red line) and solvent (blue line) method represent that the β -barrel structures were preserved after the solvent based crystallization process, a, OmpF b, FhuA $\Delta C/\Delta 4L$ c, αHL . All quantitative analyses were fitted by multivariate secondary structure analysis from JASCO software (JWMVS-529 Multivariate SSE analysis, JASCO). Generally, the peak positions less than 200 nm could not be characterized due to the strong absorption of rehydration buffer at short wavelengths. The lower peaks from crystals in panels b, and c, resulted from low protein concentrations in crystal solutions and adsorption flattening optical effects but the essential features are preserved between the two self-assembly methods as described in the text.

Integration of porous channel nanosheets into scalable membranes

The formation of thin selective layers created through the deposition of 2D nanosheets on porous support membranes has been demonstrated recently for graphene oxide sheets^{56, 57} and metal-organic frameworks nanosheets^{58, 59}. Recently, we developed a modified layer-by-layer deposition technique to fabricate artificial water channel-based membranes³⁷ from 2D sheets of polymer-channel composites. This method was adapted for membrane fabrication here and MPbased membranes was first assembled into a dead-end filtration setup (Model 8010, Millipore Corp., MA) of membrane active area, 4.1 cm². In Fig. 4a, a scanning electron microscopy (SEM) micrograph demonstrates the representative deposition of a hexagonal micron-sized OmpF crystal on the surface of a track-etched polycarbonate (PC, Whatman® NucleporeTM, UK) substrate. For molecularly-thin multi-layered membrane development, selective layer stability is a critical challenge that must be addressed because the constituent layers are susceptible to delamination if the interlayer interactions are weak⁶⁰. Therefore, to confer stability to the membranes, PB-PEO BCPs with carboxylic acid-terminated PEO blocks were used in crystal formation. The carboxylic acid groups were chemically crosslinked with the amines of the polyethylenimine (PEI) polymer layers deposited between each layer of nanosheets (Fig. 1c, see SI for details)³⁷. To optimize the membrane fabrication process, OmpF-membranes prepared with different number of deposition layers were tested and it was identified that at least six-repeated depositions (6-layered membranes) were required to achieve ~100% coverage of nanosheets on the support membranes, as seen in Fig 4a-c where all support pores are covered as well as from the cross-sectional overview of a cryogenic scanning electron microscopy (cryo-SEM, Fig. 4b). This claim is further supported

by the transport characteristics of the membranes, which are discussed in more detail in the following section. The selective layers of 6-layered OmpF-membranes were around 250 nm thick (Fig. 4c), which is close to the theoretically calculated thickness, ~200 nm (see SI for details). High-resolution scanning TEM (STEM) and energy dispersive spectroscopy (EDS) mapping suggested that enriched nitrogen species were present at or near the surface and sulfur elements only appeared at the bottom support, indicating the formation of the OmpF-nanosheet selective layers on top of the a commercial polyethersulfone (PES, MP005, Microdyn NadirTM) support. Some nitrogen species shown within the PES (MP005) membrane may be attributed to residual poly(vinyl pyrrolidone) used as additive during manufacturing of PES ultrafiltration membrane, the likely penetration of the N-containing chemical crosslinkers throughout the fabrication process and some permeation of small OmpF 2D nanosheets or proteins during the pressure-driven deposition process. (Figs. 4d-f). Further demonstration of OmpF-membrane deposited on an aluminum oxide (Al₂O₃)-based membrane (0.02 µm Anodisc, Whatman®) showed a clear boundary between OmpF-BCP nanosheet selective layers (nitrogen enriched) and Al₂O₃ substrates (aluminum enriched) by EDS mapping (Figs. 4g-i). The fabrication of OmpF 2D nanosheets on polymeric and inorganic substrates indicates the versatility of the layer-by-layer fabrication process employed.

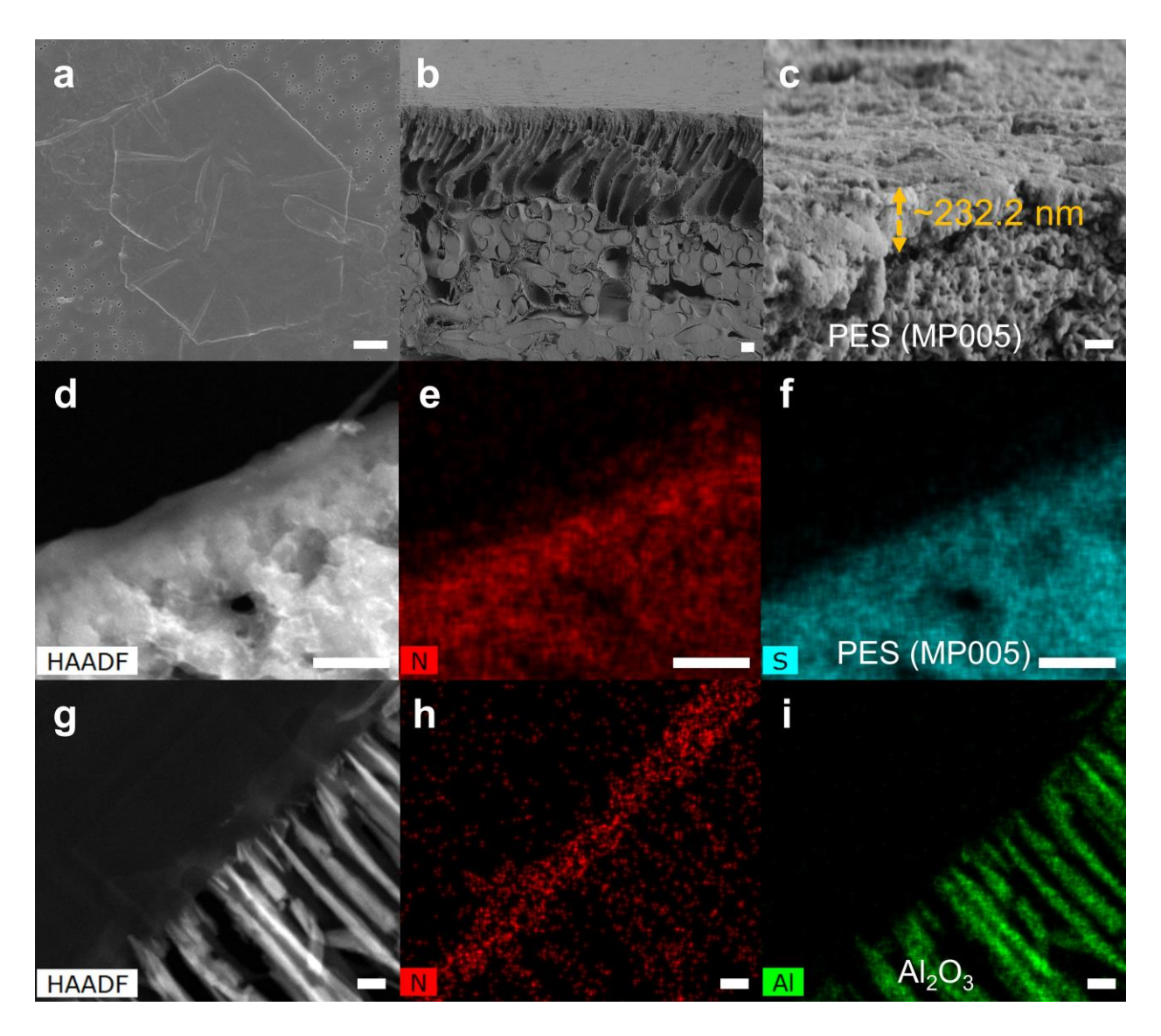


Fig. 4 | 2D OmpF nanosheets can be assembled on a polycarbonate (PC) and polyethersulfone (PES, MP005) substrate. a, Top view of a scanning electron microscopy (SEM) image of a single OmpF crystal on a PC support. The scale bar is 1 μ m. b, Overview of a cross-sectional Cryo-SEM image of OmpF 2D nanosheets on a PES substrate. The scale bar is 20 μ m. c, Cross-sectional Cryo-SEM image of a deposited selective layer of OmpF nanosheets on a PES (MP005) substrate, thickness of OmpF-embedded scalable membrane was measured at 232.2 \pm 24.8 nm. High-angle annular dark field (HAADF) STEM image of OmpF 2D nanosheets fabricated on the d, PES (MP005) substrate with elemental maps of e, nitrogen (red) and f, sulfur (cyan) and on the g, aluminum oxide substrate with elemental maps of h, nitrogen (red) and i, aluminum (green). The scale bar is 200 nm.

Membrane performance of β-barrel channel protein-BCPs biomimetic membranes

Membrane performance was characterized by measuring water permeation rates and solute rejection for a series of small molecular weight dyes in a dead-end filtration setup. The three β -barrel channel protein-embedded membranes exhibited unique small molecule separation performance with high water permeation rates compared to current commercial membranes. The MWCOs of these membranes were characterized by reporting the MW of the solute that was

rejected at 90% under standard operating conditions (Supplementary Table 2). The rejection properties of OmpF 2D nanosheet-embedded membranes reached the expected MWCO as more nanosheet layers were deposited (Supplementary Fig. 4). Specifically, the MWCOs of membranes with 6-layers of nanosheets deposited were ~470 Da and ~500 Da for membranes with nanosheets prepared by the dialysis method and the solvent method, respectively. These values are close to the exclusion limit of native OmpF proteins of ~500-600 Da, determined using an in vitro vesicle reconstitution approach with radioactive hydrophilic solutes^{61,61}. These results demonstrate that OmpF 2D crystal-embedded selective layers were successfully fabricated on a porous PES support and maintained their expected transport performance. Additionally, the performances of the OmpF crystal-membranes formed with dialysis and solvent methods were nearly identical as discussed subsequently. The other two channel protein-based scalable membranes also manifest sharp and unique exclusion limits of \sim 920 Da and \sim 1100 Da for α HL (dialysis) and FhuA Δ C/ Δ 4L (dialysis) membranes, respectively (Fig. 5a and Supplementary Fig. 5). Membranes with 2D sheets created using the solvent method exhibit similar MWCOs (Supplementary Figs. 6a, b). These molecular exclusion limits also confirm that channel proteins conserve their specific pore geometries in BCP membrane matrices with previously proposed MWCO of less than 2,000 Da for FhuA $\Delta C/\Delta 4L$ by poly(ethylene glycol)s (PEGs) partitioning and transport in a patch clamp set up¹⁶ as well as the region of 1,000 to 4,000 Da for αHL^{62-64} .

In addition to specific dye selectivity, these channel protein-based membranes can have other potential applications (**Supplementary Table 4**). For example, α HL-based membrane was shown to be capable of filtering virus particles (MS2 bacteriophage) with >4 log (or >99.99%) removal efficiency with applied pressure of 5 psi, meet the water treatment US EPA requirement, a performance on a par with commercial nanofiltration membranes, but need to be operated at the pressure of 50 psi (**Supplementary Fig. 7a** and see SI for details). Furthermore, only α HL membrane can also be used for 100-fold concentration of virus stock solutions with a recovery of ~80% whereas the commercial membrane does not offer this capability (**Supplementary Fig. 7b**).

In addition to demonstrating tailored selectivity consistent with the channel protein pore size, the three channel protein-embedded membranes also demonstrated rapid and stable water permeation with applied pressure of 5 psi. Comparatively, commercial membranes with similar MWCOs of ~1,000 Da, NP010 (Microdyn NadirTM) and GE (OsmonicsTM GE) had to be tested at an applied pressure of 50 psi to show appreciable flux (**Fig. 5b**). Data on stability and performance as the number of layers of crystal deposition was increased was also collected to decide on a 6-layer deposition (**Supplementary Fig. 8**) and these membranes were found to be stable with applied pressure of ~30 psi, which might be upper limit pressure for a layer-by-layer membranes in this study (**Supplementary Fig. 9-12**). However, given the very high permeability of these membranes, we do not think these pressures are something that might be expected to be used in practice for such membranes due to the high concentration polarization and fouling that may result at high fluxes that would correspond to higher pressures being used^{65, 66}.

The water permeability of three β -barrel channel protein-embedded biomimetic membranes were $\sim 293 \pm 51$ LMH bar⁻¹ for OmpF (dialysis), 724.5 ± 225.9 LMH bar⁻¹ for FhuA $\Delta C/\Delta 4L$ (dialysis), and $1,092 \pm 79.4$ LMH bar⁻¹ for αHL (dialysis)-based scalable membranes (mean \pm s.d., n = 3) (Fig. 5c). Membranes with 2D sheets created using the solvent method also demonstrated similar water permeabilities (Supplementary Fig. 5c). These 6-layered protein composite membranes prepared using dialysis and solvent methods showed equivalent membrane

performance in terms of separation properties (MWCO) and permeability indicating that the β -barrel pore structures and their function were preserved. These results recapitulate the advantages of solvent method over dialysis, especially from the perspective of process time and cost efficiency for membrane development.

The theoretical OmpF-membrane permeability was estimated at ~86.7 LMH bar-based on OmpF single porin permeability², its channel packing density from hexagonal crystal structure, as well as PB-PEO block copolymer permeability³⁷ (see SI for details). The remarkable agreement within a few folds between theoretical and experimental permeability, which were obtained from experiments spanning orders of magnitude length scales from the molecular scale to practicerelevant filtration scales, indicates successful integration of channel proteins into scalable membranes. The expected higher permeability of membranes constructed with the larger sized channels (FhuA and □HL) is also of the right scale when compared to the OmpF channels (their molecular permeability has not been characterized to the level that OmpF has been). The lower permeability for the higher pore size FhuA $\Delta C/\Delta 4L$ -based membrane compared to $\Box HL$ may be a result of molecular interactions between water molecules and the pore wall which could have a higher impact than mere pore size at these nm length scales. As shown in the Supplementary Table 3, the values of inner pore-wall hydrophobicity (see SI for details), as indicated by $\Delta G_{transfer}^{water \rightarrow ethanol}$ values⁶⁷ (from the Kyte-Doolittle (KD) hydrophobicity scale), for FhuA $\Delta C/\Delta 4L$ (-70.4 kcal/mol) is lower than that of αHL (-84.3 kcal/mol). This indicates that the inner pore of FhuA ΔC/Δ4L is less hydrophobic and more likely to form more hydrogen-bonded interaction with the permeating water molecules, which further lead to the lower permeability compared to αHL proteins.

MP-based membranes exhibited orders of magnitude higher permeabilities relative to state-of-the-art polymeric NF membranes (**Fig. 5c**). For accurate comparison, two commercial membranes, NP010 and GE, which are rated to have MWCOs of ~1000 Da, were tested with the same experimental setup for their permeability values. Even though the commercial membranes had MWCO values similar to the value determined for the protein membranes, the water permeability of the control GE and NP010 membranes were 1.6 ± 0.6 LMH bar⁻¹ and 13.2 ± 0.5 LMH bar⁻¹, respectively compared to over ~300 LMH bar⁻¹ for all the MP-based membranes tested in this study.

In addition to assembling our MP-based membranes in a small Amicon Stirred Cell Model 8010 (Millipore Corp., MA) which accepts membranes of 4.1 cm² area, we also deposited the 6-layered αHL nanosheets into the larger filtration setup, Amicon Stirred Cell Model 8400 (Millipore Corp., MA) with a filtration area of 41.8 cm², as demonstrated in the **Supplementary Fig. 13a**. This three-inch diameter (41.8 cm²) αHL membrane demonstrated rapid and stable water permeation with applied pressure of 5 psi (**Supplementary Fig. 13b**) with a water permeability of ~1,178 LMH bar¹ (**Supplementary Fig. 13c**), similar to that of 4.1 cm² membrane. Additionally, this αHL membrane also maintained 98% rejection of fluorescent dextran, 3 KDa and 39% rejection of acid fuchsin as observed with the 4.1 cm² membrane. Furthermore, an *in situ* deposition technique was applied to deposit αHL-embedded membrane on a PES (MP005) substrate in a cross flow cell (CF016D, Sterilitech) with a ~14.4 cm² membrane area (**Supplementary Fig. 14 a-d**). The water permeability was measured to be 1,358.2±144.0 LMH bar¹¹ for control PES (MP005) membrane and 1,325.6±43.8 LMH bar¹¹ for αHL-embedded membrane, which is similar in performance to that obtained during dead-end filtration (1,092 ±

79.4 LMH bar⁻¹) (**Supplementary Fig. 14 e**). The water permeability was maintained for more than 120 hours before we conducted dye rejection tests (**Supplementary Fig. 14 f and 14 g**) which resulted in similar rejection profiles as in the dead-end tests. The rejection properties included 99.1% rejection for Blue dextran (5 KDa), 93.9% for Fluorescent Dextran (3 KDa) and 13.1 % for Acid Fuchsin, which are similar to those obtained from concentration polarization corrected dead-end filtration cell results.

The extremely high permeability of the protein-based membranes led us to ask if the porous support membranes were well matched to our active filtration layer. There have been reports in literature indicating that the design of membrane support has a major impact on the performance of composite membranes⁶⁸. Most experiments in this work were conducted with a PES (MP005) support with a measured permeability of 1,296 \pm 64 LMH bar⁻¹. While this seems to be a reasonably high permeability for our OmpF composite membranes to be built on (with a permeability of ~300 LMH bar⁻¹), we suspected that this support might be limiting for the αHL nanosheets-embedded membranes (permeability of $1,092 \pm 79.4$ LMH bar⁻¹). When α HL nanosheets were supported on a more permeable 0.03 μ m PES support (3,039 \pm 136 LMH bar⁻¹, (Sterlitech Corp., WA), the composite membrane (designated αHL*) demonstrated an even higher water permeance of $2{,}107 \pm 235$ LMH bar⁻¹, while maintaining a similar MWCO of $1{,}030$ Da as that with the less permeable support. A similar trend in permeability was observed when OmpF crystals were supported on less permeable track etched polycarbonate (PC) support membranes compared to the PES (MP005) membranes (Supplementary Fig. 15a). Thus, for these highly permeable selective layers derived from 2D MP nanosheets, support selection and design are of critical importance.

Extensive comparison of OmpF, α HL, and FhuA Δ C/ Δ 4L-based membranes to commercial membranes highlights significantly enhanced membrane performance of channel-based membranes (**Fig. 6**). MP channel-based membranes manifested ~20 to 1,000-fold enhanced water productivity over commercial membranes as a result of high pore packing densities of protein channels in the self-assembled 2D crystals and nanosheets. Specifically, the OmpF-membrane has ~20 times greater pure water permeability than the highest permeability commercial membrane, NF270 (water permeability of 14.7 \pm 0.7 LMH bar⁻¹ with MWCO of 400 Da) and ~100 times greater permeability than N30F previously tested on the same experimental setup in our lab³⁷. In the separation range between 500 Da to 1,200 Da, α HL nanosheets supported on PES (Sterlitech Corp., WA) membrane demonstrates almost 1,000-fold water permeability of ~ 2000 LMH bar⁻¹ over the GE membrane (water permeability of 1.5 \pm 0.4 LMH bar⁻¹ with MWCO ~1,100 Da).

Remarkably, OmpF-membranes show approximately an order of magnitude higher permeability than our recently reported artificial channel based membranes of a similar MWCO (PAP[5] membranes, MWCO ~ 500 Da)³⁷. This corresponds to the tradeoff between expected two order higher single channel permeability of OmpF² compared to PAP[5] channels^{5,37} and the one order lower effective cross sectional area of MPs compared to artificial channels. These two opposing trend correspond to the one order increase in permeability of OmpF membranes compared to PAP[5] membranes created using a similar approach. Compared to current research membranes (**Supplementary Table 5**), for the OmpF size range of ~ 500 Da, the OmpF membrane has ~1.5 times greater pure water permeability than the highest permeability research membrane, Tp-Bpy thin film (water permeability of 211 LMH bar⁻¹ with MWCO of 585 Da) which is slightly

higher in pore size than our membrane. In the separation range between 800 Da to 2,400 Da, membranes in this study represented by αHL nanosheets supported on PES, demonstrates almost 45-fold water permeability of $\sim 2,000$ LMH bar⁻¹ over the Torlon & sPPSU membrane (water permeability of 82.5 LMH bar⁻¹ with MWCO $\sim 1,000$ Da).

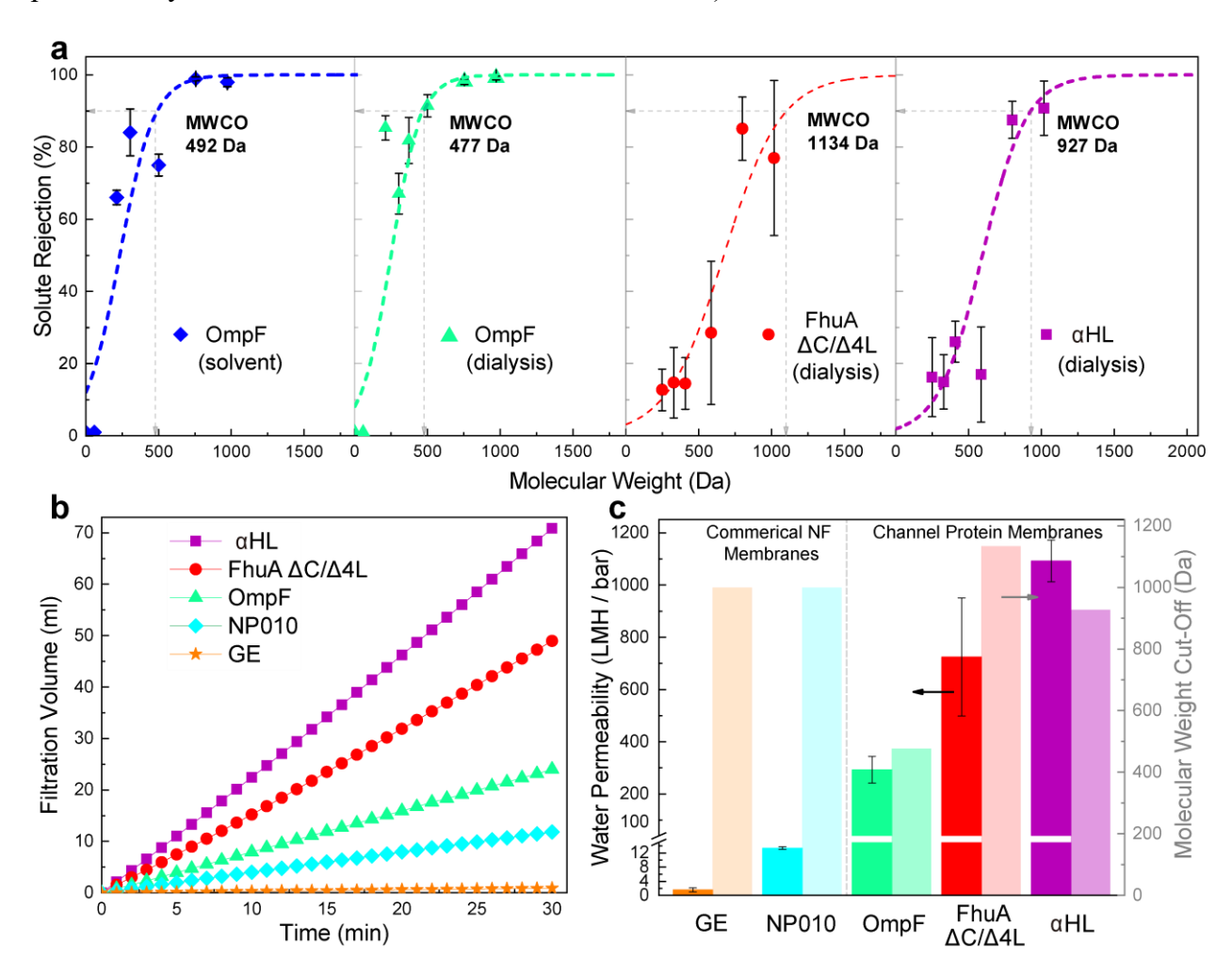


Fig. 5 | Three β-barrel channel protein-copolymer based scalable membranes demonstrate distinct molecular separations and enhanced pure water permeability compared with current commercial membranes. a, The molecular weight cutoffs (MWCOs) measured were ~490 Da, ~480 Da, ~930 Da and ~1,130 Da for OmpF (solvent), OmpF (dialysis), αHL (dialysis), FhuA Δ C/ Δ 4L (dialysis) channel protein-embedded biomimetic membranes, respectively, as determined from filtration of dyes of various molecular weights and fitting to a sigmoidal model⁶. b, Plot of water filtration volume vs time of OmpF, αHL, FhuA Δ C/ Δ 4L (dialysis) based biomimetic membranes (filtration under 5 psi), NP010 and GE commercial membranes (filtration under 50 psi). c, The water permeability of three β-barrel channel protein-embedded biomimetic membranes were 293 \pm 51 LMH bar⁻¹, 724.5 \pm 225.9 LMH bar⁻¹, and 1,092 \pm 79.4 LMH bar⁻¹ for OmpF (dialysis), FhuA Δ C/ Δ 4L (dialysis), αHL (dialysis), demonstrating one or two order of magnitude higher permeability than commercial membranes.

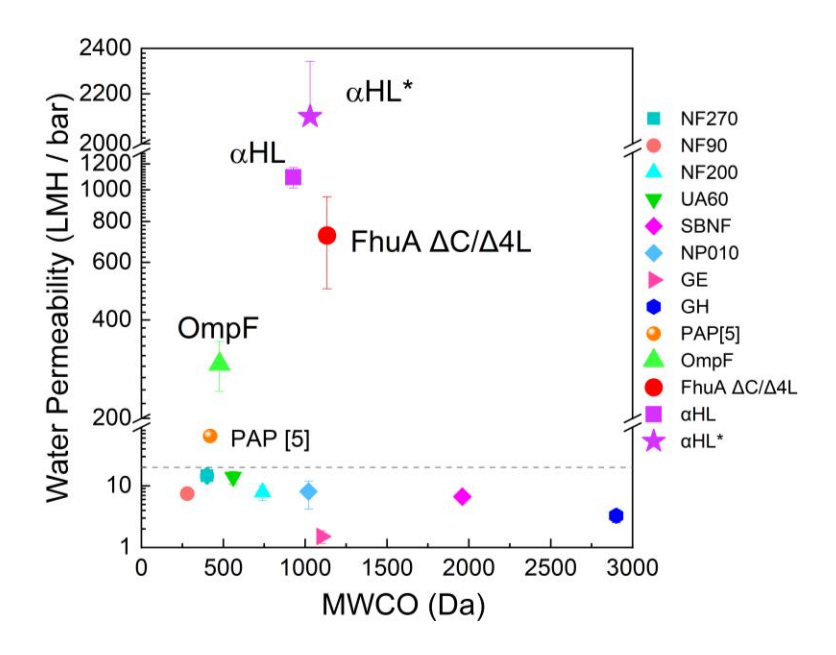


Fig. 6 | Comparison of water permeability (LMH bar⁻¹) and MWCO (Da) of membrane protein based membranes with commercial NF or UF membranes tested in the same experimental setup. The results clearly demonstrate that the β -barrel channel protein-based membranes have an order to almost three orders of magnitude higher permeability than commercial NF membranes with the MWCO ratings from 50 Da to 3,000 Da. α HL* represents composite membranes with α HL nanosheets supported on a highly permeable 0.03 μ m PES (Sterlitech Corp., WA) support as compared to α HL indicating membranes supported on a lower permeability MP005 PES support used for all membranes. The dashed line (at a water permeability value of 20 LMH bar⁻¹) represents the upper limits of water permeability of current commercial membranes in the challenging sub nanometer to few nanometer separation ranges. The commercial membranes were tested with additional 200 mM NaCl to screen out charge effects.

Conclusions and outlook

In summary, pore-forming membrane protein channels, OmpF, α HL and FhuA Δ C/ Δ 4L, were successfully integrated into membranes at close to practice-relevant centimeter size scales, along with development of a preparation method to create highly packed channel-nanosheets using a rapid (2-hour) organic solvent-based technique. The functionality and structure integrity of membrane protein channels in 2D crystals or nanosheets have been preserved. Resulting biomimetic membranes demonstrated one to three orders of magnitude higher water permeability than commercial nanofiltration membranes and 1.5 to 45 times higher permeability than the latest research membranes with similar separation ratings while maintaining their expected high small molecule solute selectivity. This result implies that membrane performance could be precisely designed through functional channel modification and their integration into membranes. Additionally, these biomimetic membranes can be applied at low pressures (~5 psi) to maintain high fluxes, thus reducing power consumption substantially. This approach of combining channel proteins and BCPs through scalable self-assembly and further development of the layer-by-layer MP membrane fabrication technique highlights the promise of developing MP-based biomimetic membranes for future applications where the exquisite specificity and functionality of channel proteins can provide effective small molecule separations.

Acknowledgements

The authors acknowledge financial support from the National Science Foundation (NSF) CAREER grant (CBET-1552571) and NSF grant CBET- 1804836 to MK for this work.

References

- 1. Kumar, M., Grzelakowski, M., Zilles, J., Clark, M., Meier, W. Highly permeable polymeric membranes based on the incorporation of the functional water channel protein Aquaporin Z. *Proc. Natl. Acad. Sci. USA*, **104**(52), 20719-20724 (2007).
- 2. Chowdhury, R., *et al.* PoreDesigner for tuning solute selectivity in a robust and highly permeable outer membrane pore. *Nat. Commun.*, **9**(1), 3661 (2018).
- 3. Ren, T.W., *et al.* Membrane Protein Insertion into and Compatibility with Biomimetic Membranes. *Advanced Biosystems*, **1**(7), 1700053 (2017).
- 4. Kumar, M., Habel, J.E., Shen, Y.-x., Meier, W.P., Walz, T. High-density reconstitution of functional water channels into vesicular and planar block copolymer membranes. *J. Am. Chem. Soc.*, **134**(45), 18631-18637 (2012).
- 5. Shen, Y.-x., *et al.* Highly permeable artificial water channels that can self-assemble into two-dimensional arrays. *Proc. Natl. Acad. Sci. USA*, **112**(32), 9810-9815 (2015)
- 6. Shen, Y.-x., *et al.* Achieving high permeability and enhanced selectivity for Angstromscale separations using artificial water channel membranes. *Nat. Commun.*, **9**(1), 2294 (2018).
- 7. Song, W., Lang, C., Shen, Y.-x., Kumar, M. Design considerations for artificial water channel–based membranes. *Ann. Rev. Mater. Res.*, **48**, 57-82 (2018).
- 8. Kocsis, I., Sun, Z., Legrand, Y.M., Barboiu, M. Artificial water channels—deconvolution of natural Aquaporins through synthetic design. *npj Clean Water*, **1**(1), 13 (2018).
- 9. Hinds, B.J., Chopra, N., Rantell, T., Andrews, R., Gavalas, V., Bachas, L.G. Aligned multiwalled carbon nanotube membranes. *Science*, **303**(5654), 62-65 (2004).
- 10. Park, H.B., Kamcev, J., Robeson, L.M., Elimelech, M., Freeman, B.D. Maximizing the right stuff: The trade-off between membrane permeability and selectivity. *Science*, **356**(6343), eaab0530 (2017).
- 11. Mohammad, A.W., Teow, Y., Ang, W., Chung, Y., Oatley-Radcliffe, D., Hilal, N. Nanofiltration membranes review: Recent advances and future prospects. *Desalination*, **356**, 226-254 (2015).
- 12. Artuğ, G., Roosmasari, I., Richau, K., Hapke, J. A comprehensive characterization of commercial nanofiltration membranes. *SS&T*, **42**(13), 2947-2986 (2007).
- 13. Shen, Y.X., Saboe, P.O., Sines, I.T., Erbakan, M., Kumar, M. Biomimetic membranes: A review. *J. Membr. Sci.*, **454**, 359-381 (2014).

- 14. Duong, P.H.H., *et al.* Planar biomimetic aquaporin-incorporated triblock copolymer membranes on porous alumina supports for nanofiltration. *J. Membr. Sci.*, **409**, 34-43 (2012).
- 15. Wang, M., Wang, Z., Wang, X., Wang, S., Ding, W., Gao, C. Layer-by-layer assembly of aquaporin Z-incorporated biomimetic membranes for water purification. *Environ. Sci. Technol.*, **49**(6), 3761-3768 (2015).
- 16. Niedzwiecki, D.J., Mohammad, M.M., Movileanu, L. Inspection of the engineered fhua δc/δ4l protein nanopore by polymer exclusion. *Biophys. J.*, **103**(10), 2115-2124 (2012).
- 17. Blanazs, A., Armes, S.P., Ryan, A.J. Self-assembled block copolymer aggregates: from micelles to vesicles and their biological applications. *Macromol. Rapid Commun.*, **30**(4-5), 267-277 (2009).
- 18. Helix-Nielsen, C. Biomimetic Membranes as a Technology Platform: Challenges and Opportunities. *Membranes (Basel)*, **8**(3), 44 (2018).
- 19. Song, W., Tu, Y.M., Oh, H., Samineni, L., Kumar, M. Hierarchical optimization of high performance biomimetic and bioinspired membranes. *Langmuir*, (2018).
- 20. Tang, C.Y., Zhao, Y., Wang, R., Helix-Nielsen, C., Fane, A.G. Desalination by biomimetic aquaporin membranes: Review of status and prospects. *Desalination*, **308**, 34-40 (2013).
- 21. Tamm, L.K., Arora, A., Kleinschmidt, J.H. Structure and assembly of beta-barrel membrane proteins. *J. Biol. Chem.*, **276**(35), 32399-32402 (2001).
- 22. Wimley, W.C. The versatile β-barrel membrane protein. *Curr. Opin. Struct. Biol.*, **13**(4), 404-411 (2003).
- 23. Cowan, S.W., *et al.* Crystal structures explain functional properties of two E. coli porins. *Natur*, **358**(6389), 727-733 (1992).
- 24. Phale, P.S., *et al.* Stability of trimeric OmpF porin: the contributions of the latching loop L2. *Biochemistry*, **37**(45), 15663-15670 (1998).
- 25. Lee, A.G. Lipid-protein interactions in biological membranes: a structural perspective. *Biochim. Biophys. Acta*, **1612**(1), 1-40 (2003).
- Wong, D., Jeon, T.J., Schmidt, J. Single molecule measurements of channel proteins incorporated into biomimetic polymer membranes. *Nanot*, **17**(15), 3710-3717 (2006).
- 27. Palivan, C.G., Goers, R., Najer, A., Zhang, X., Car, A., Meier, W. Bioinspired polymer vesicles and membranes for biological and medical applications. *Chem. Soc. Rev.*, **45**(2), 377-411 (2016).

- 28. Klara, S.S., *et al.* Magnetically Directed Two-Dimensional Crystallization of OmpF Membrane Proteins in Block Copolymers. *J. Am. Chem. Soc.*, **138**(1), 28-31 (2016).
- 29. Cowan, S., *et al.* The structure of OmpF porin in a tetragonal crystal form. *Structure*, **3**(10), 1041-1050 (1995).
- 30. Pebay-Peyroula, E., Garavito, R., Rosenbusch, J., Zulauf, M., Timmins, P. Detergent structure in tetragonal crystals of OmpF porin. *Structure*, **3**(10), 1051-1059 (1995).
- 31. Haltia, T., Freire, E. Forces and Factors That Contribute to the Structural Stability of Membrane-Proteins. *Biochim. Biophys. Acta*, **1228**(1), 1-27 (1995).
- White, S.H., Wimley, W.C. Membrane protein folding and stability: physical principles. *Annu. Rev. Biophys. Biomol. Struct.*, **28**(1), 319-365 (1999).
- 33. Kleffel, B., Garavito, R.M., Baumeister, W., Rosenbusch, J.P. Secondary structure of a channel-forming protein: porin from E. coli outer membranes. *EMBO J.*, **4**(6), 1589-1592 (1985).
- 34. Mohammad, M.M., Howard, K.R., Movileanu, L. Redesign of a plugged β-barrel membrane protein. *J. Biol. Chem.*, **286**(10), 8000-8013 (2011).
- 35. Gouaux, J.E., *et al.* Subunit stoichiometry of staphylococcal alpha-hemolysin in crystals and on membranes: a heptameric transmembrane pore. *Proc. Natl. Acad. Sci. USA*, **91**(26), 12828-12831 (1994).
- 36. Jap, B.K., et al. 2D crystallization: from art to science. *Ultmi*, **46**(1-4), 45-84 (1992).
- 37. Shen, Y.-x., *et al.* Achieving high permeability and enhanced selectivity for Angstromscale separations using artificial water channel membranes. *Nat. Commun.*, **9**, (2018).
- 38. Perry, M., Madsen, S., Jørgensen, T., Braekevelt, S., Lauritzen, K., Hélix-Nielsen, C. Challenges in commercializing biomimetic membranes. *Membranes*, **5**(4), 685-701 (2015).
- 39. Kowal, J., Zhang, X.Y., Dinu, I.A., Palivan, C.G., Meier, W. Planar Biomimetic Membranes Based on Amphiphilic Block Copolymers. *ACS Macro Lett.*, **3**(1), 59-63 (2014).
- 40. Belegrinou, S., Dorn, J., Kreiter, M., Kita-Tokarczyk, K., Sinner, E.K., Meier, W. Biomimetic supported membranes from amphiphilic block copolymers. *Soft Matter*, **6**(1), 179-186 (2010).
- 41. Jin, H., *et al.* Highly stable and self-repairing membrane-mimetic 2D nanomaterials assembled from lipid-like peptoids. *Nat. Commun.*, 7, 12252 (2016).

- 42. Kumar, M., Habel, J.E., Shen, Y.X., Meier, W.P., Walz, T. High-density reconstitution of functional water channels into vesicular and planar block copolymer membranes. *J. Am. Chem. Soc.*, **134**(45), 18631-18637 (2012).
- 43. Biyani, N., *et al.* Focus: The interface between data collection and data processing in cryo-EM. *J. Struct. Biol.*, **198**(2), 124-133 (2017).
- 44. Hasler, L., Heymann, J.B., Engel, A., Kistler, J., Walz, T. 2D crystallization of membrane proteins: rationales and examples. *J. Struct. Biol.*, **121**(2), 162-171 (1998).
- 45. Signorell, G.A., Kaufmann, T.C., Kukulski, W., Engel, A., Rémigy, H.-W. Controlled 2D crystallization of membrane proteins using methyl-β-cyclodextrin. *J. Struct. Biol.*, **157**(2), 321-328 (2007).
- 46. Dorset, D.L., Engel, A., Haner, M., Massalski, A., Rosenbusch, J.P. Two-dimensional crystal packing of matrix porin. A channel forming protein in Escherichia coli outer membranes. *J. Mol. Biol.*, **165**(4), 701-710 (1983).
- 47. Ferro, M., *et al.* Organic solvent extraction as a versatile procedure to identify hydrophobic chloroplast membrane proteins. *Electrophoresis*, **21**(16), 3517-3526 (2000).
- 48. Gessmann, D., *et al.* Improving the resistance of a eukaryotic β-barrel protein to thermal and chemical perturbations. *J. Mol. Biol.*, **413**(1), 150-161 (2011).
- 49. Panganiban, B., et al. Random heteropolymers preserve protein function in foreign environments. *Science*, **359**(6381), 1239-1243 (2018).
- 50. Klara, S.S., *et al.* Magnetically directed two-dimensional crystallization of OmpF membrane proteins in block copolymers. *J. Am. Chem. Soc.*, **138**(1), 28-31 (2015).
- 51. Kelly, S.M., Jess, T.J., Price, N.C. How to study proteins by circular dichroism. *Biochim. Biophys. Acta*, **1751**(2), 119-139 (2005).
- 52. Manzo, G., *et al.* Enhanced amphiphilic profile of a short β-stranded peptide improves its antimicrobial activity. *PLoS One*, **10**(1), e0116379 (2015).
- 53. Efremov, R.G., Sazanov, L.A. Structure of Escherichia coli OmpF porin from lipidic mesophase. *J. Struct. Biol.*, **178**(3), 311-318 (2012).
- 54. Bulheller, B.M., Hirst, J.D. DichroCalc—circular and linear dichroism online. *Bioinformatics*, **25**(4), 539-540 (2009).
- 55. Wallace, B.A., Teeters, C.L. Differential absorption flattening optical effects are significant in the circular dichroism spectra of large membrane fragments. *Biochemistry*, **26**(1), 65-70 (1987).

- 56. Huang, H.B., Ying, Y.L., Peng, X.S. Graphene oxide nanosheet: an emerging star material for novel separation membranes. *Journal of Materials Chemistry A*, **2**(34), 13772-13782 (2014).
- 57. Hu, M., Mi, B. Enabling graphene oxide nanosheets as water separation membranes. *Environ. Sci. Technol.*, **47**(8), 3715-3723 (2013).
- 58. Peng, Y., *et al.* Metal-organic framework nanosheets as building blocks for molecular sieving membranes. *Science*, **346**(6215), 1356-1359 (2014).
- 59. Liu, G., Jin, W., Xu, N. Two-Dimensional-Material Membranes: A New Family of High-Performance Separation Membranes. *Angew. Chem. Int. Ed. Engl.*, **55**(43), 13384-13397 (2016).
- 60. Thebo, K.H., Qian, X., Zhang, Q., Chen, L., Cheng, H.M., Ren, W. Highly stable graphene-oxide-based membranes with superior permeability. *Nat. Commun.*, **9**(1), 1486 (2018).
- 61. Nikaido, H., Saier, M.H. Transport Proteins in Bacteria Common Themes in Their Design. *Science*, **258**(5084), 936-942 (1992).
- 62. Bhakdi, S., Tranum-Jensen, J. Alpha-toxin of Staphylococcus aureus. *Microbiol. Rev.*, **55**(4), 733-751 (1991).
- 63. Bezrukov, S.M., Vodyanoy, I., Brutyan, R.A., Kasianowicz, J.J. Dynamics and free energy of polymers partitioning into a nanoscale pore. *Macromolecules*, **29**(26), 8517-8522 (1996).
- 64. Bhakdi, S., Muhly, M., Fussle, R. Correlation between Toxin Binding and Hemolytic-Activity in Membrane Damage by Staphylococcal Alpha-Toxin. *Infect. Immun.*, **46**(2), 318-323 (1984).
- 65. Zhang, R., *et al.* Antifouling membranes for sustainable water purification: strategies and mechanisms. *ChSRv*, **45**(21), 5888-5924 (2016).
- 66. Jang, E.-S., *et al.* Influence of concentration polarization and thermodynamic non-ideality on salt transport in reverse osmosis membranes. *J. Membr. Sci.*, **572**, 668-675 (2019).
- 67. Kyte, J., Doolittle, R.F. A simple method for displaying the hydropathic character of a protein. *J. Mol. Biol.*, **157**(1), 105-132 (1982).
- 68. Jegal, J., Min, S.G., Lee, K.H. Factors affecting the interfacial polymerization of polyamide active layers for the formation of polyamide composite membranes. *J. Appl. Polym. Sci.*, **86**(11), 2781-2787 (2002).